Research Article Vol. 32, No. 5 / 26 Feb 2024 / Optics Express 7391
Optics EXPRESS

High-sensitivity and high-speed measurements of ultrashort pulses as short as 74 fs at 1.9 µm using a GRENOUILLE device

DANIIL BATOV,[1,*] VASILII VOROPAEV,[1] RANA JAFARI,[2] SELCUK AKTURK,[2] VLADIMIR LAZAREV,[1] VALERIY KARASIK,[1] RICK TREBINO,[3] AND MIKHAIL TARABRIN[1]

[1]Science and Education Center for Photonics and IR-Technology, Bauman Moscow State Technical University, Moscow, 105005, Russia
[2]Swamp Optics LLC, 6300 Powers Ferry Road, Suite 600-345, Atlanta, Georgia 30339, USA
[3]School of Physics, Georgia Institute of Technology, 837 State Street, Atlanta, Georgia 30332, USA
*daniilbatov@gmail.com

Abstract: Ultrashort laser pulse sources in the wavelength range of 1.8 to 2 µm have many potential applications including medicine, materials processing, and sensing. In the use of such lasers, a crucial task is to measure their pulse's temporal intensity and phase. Such measurement devices are most useful when they are simple to build and operate and also have high speed and high sensitivity. The GRENOUILLE measurement device with few components, no moving parts, sensitivity of hundreds of picojoules, and measurement speed of hundreds of milliseconds, is commonly used to solve this problem at other wavelengths. In this paper, the measurement of ultrashort pulses by a GRENOUILLE device, developed using a silicon matrix sensor, for pulses in the wavelength range of 1.8 to 2 µm has been demonstrated. It is shown that ultrashort pulses with durations of 74 to 900 fs and a maximum spectral FWHM of 85 nm can be measured with this device. The recently developed ultra-reliable RANA approach was used for pulse retrieval from the measured traces. The device's performance was validated by comparing its measurements with those obtained by the robust FROG technique.

1. Introduction

Thulium-doped ultrafast fiber lasers are capable of operating over a wide spectral range from 1.7 to 2 µm [1–3], which accounts for the wide range of potential applications of such sources in various areas of life [4]. For example, the intense water absorption peak at 1.93 µm [5] makes the femtosecond thulium-doped fiber laser a good candidate for use as a precision surgical instrument with minimal damage to surrounding tissues [6]. At the same time, there is a biological window of transparency in the wavelength range from 1.6 to 1.87 µm, which makes it possible to study biological tissues by optical coherence tomography and to diagnose diseases [7]. Using an ultrafast thulium-doped fiber laser and highly nonlinear media, it is possible to obtain radiation in the mid-IR range (2-20 µm) characterized by a large number of absorption lines of various substances, which can be used for their detection [8–14]. Other applications include polymer processing [15], in-volume processing of IR materials (silicon, germanium) [16], high frequency generation [17,18], and sensing [19].

Unfortunately, pulses from ultrafast fiber lasers can vary in undesirable ways due to fluctuations in temperature, pump power, and the polarization properties of the fiber. Moreover, fiber amplifiers often produce ultrashort pulses (USPs) with short duration, and high energy, but in addition, a set of low-intensity satellite pulses with longer durations and significantly spaced in time. This considerably complicates their use. It also complicates their measurement using robust methods such as FROG due to the need to obtain high temporal and spectral resolution, varying

#512303 https://doi.org/10.1364/OE.512303
Journal © 2024 Received 7 Dec 2023; revised 2 Feb 2024; accepted 2 Feb 2024; published 15 Feb 2024

Optics EXPRESS

a delay between two pulse replicas interacting in a second harmonic generation (SHG) crystal [20,21]. As a result, most intensity and phase measurement methods are time-consuming [22]. In addition, the vast majority of such methods also require moving parts in the delay line and are difficult to assemble, align and maintain aligned. Also, these methods have low sensitivities due to the required use of very thin SHG crystals, which imposes limitations on measurements of low energy pulses, and measurement times of potentially minutes, which prevents measuring short-term fluctuations of pulse generation regimes.

The GRENOUILLE device for measuring USPs is an elegant variation on the FROG technique that was introduced more than 30 years ago [23,24]. Its primary distinguishing feature is a thick SHG crystal that generates second harmonic radiation with power orders of magnitude higher than that generated in thin crystals. This leads to significantly increased sensitivity. As a result, it can use crossed, less intense line-focused beams to map delay onto transverse position and hence achieve single-shot operation. Consequently, GRENOUILLE allows the measurement of the pulse characteristics of unstable pulse generation regimes, as its speed is only limited by the exposure time of a camera (typically milliseconds). In addition, while the measured trace is an intuitive measure of the pulse, additional time can be invested in retrieving the precise pulse intensity and phase, but this occurs after the measurement is made and has "frozen the action". Finally, the absence of moving parts in GRENOUILLE, in general, makes it quite easy to assemble, align, and operate.

The measurement of sub-20 fs to 1 ps pulses from a Ti:Sapphire laser [24] using the GRENOUILLE device and its extension to pulses with center wavelengths of 1.5 μm and 1.7 μm [25] have been demonstrated previously. However, current commercially available systems that can measure the temporal intensity and phase of a pulse at a wavelength of 1.9 μm have a thin crystal and limited sensitivity, which makes fast measurement of such mid-IR laser sources with pulse energies of about hundreds of picojoules impossible.

Fortunately, it was previously shown that the phase-matching curve of Ag_3AsS_3 crystals is ideal for GRENOUILLE pulse measurement devices in the range of 1.8 to 2 μm [25], but the measurement of pulses in this range was demonstrated experimentally only for pulses of 200 fs duration [26] (by our group), and shorter pulses could not be measured in that experiment due to the limited spectral range of that GRENOUILLE setup. Thus, the goal of the present research is to develop a GRENOUILLE device for measuring pulses of a thulium-doped fiber laser system with durations from 70 fs to 1 ps in the wavelength range of 1.8 to 2 μm. Specifically, this work demonstrates the results of the development of a measurement system that allows fast, sensitive, and reliable measurement of pulses with durations from 74 to 900 fs with a pulse energy of about 500 pJ a center wavelength of about 1.9 μm, and a maximum spectrum width at half-maximum of about 85 nm, which has been validated using the well-established FROG method, as well as a spectrometer and autocorrelator.

2. Experimental setup

Figure 1 shows three-dimensional, top, and side views of the developed GRENOUILLE device. The operating principle of GRENOUILLE has been described in great detail previously [22–24,27], so only the detailed characteristics of the components used in the setup are presented below.

An N-BK7 CL1 cylindrical lens with a 100 mm focal length focuses the laser beam into the Ag_3AsS_3 (proustite) type I (ooe) SHG crystal with a thickness in the beam direction of 3.5 mm. An N-BK7 Fresnel biprism FB with an apex angle of 160° splits the input beam into two beams that cross in space and time in the SHG crystal and provides the SHG of the USP at different pulse delays relative to itself. The apex angle of the biprism is chosen so that, for an input 20-mm beam diameter, the delay range at the full overlap of two converging beams is 6 ps.

The crystal is cut for SHG at 1.9 μm (θ = 33.7°) and it has antireflection coatings with reflectance intensities less than 2 % on the entrance face at 1800 to 2000 nm and on the exit

Optics EXPRESS

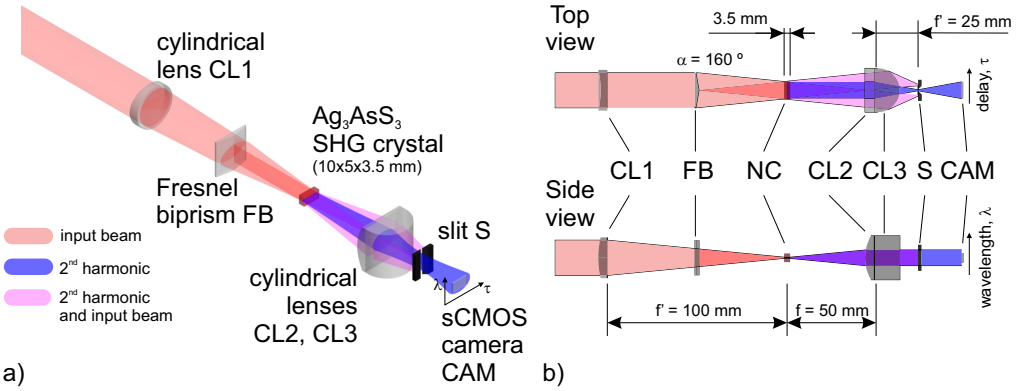

Fig. 1. Schematic of the GRENOUILLE setup for measuring the intensity and phase of USP, a) a three-dimensional view of the device, b) top and side views.

face at 900 to 1000 nm. Due to the use of a thick nonlinear crystal, the radiation of the second harmonic is spectrally spread out by angle, which provides measurement of the second harmonic spectrum [27]. On the one hand, GRENOUILLE uses the group velocity mismatch (GVM) of the fundamental and second harmonic in the crystal for spectral resolution. GVM is calculated by using the equation:

$$\mathrm{GVM} = \frac{1}{v_g^o(\lambda_0)} - \frac{1}{v_g^e(\frac{\lambda_0}{2})}, \tag{1}$$

where v_g^o, v_g^e - are the group velocities for ordinary and extraordinary rays, respectively, in m/s. For pulses with a center wavelength λ_0 of 1.9 μm, it is $5.54 \cdot 10^3$ fs/cm. On the other hand, the pulse's group velocity dispersion (GVD) determined for the full width at half maximum (FWHM) bandwidth $\Delta\lambda_{0.5}$, nm should not cause the pulse to spread in time (not to be confused with usual crystal group velocity dispersion β_2, s^2/m). The pulse's GVD can be calculated using the following equation:

$$\mathrm{GVD} = \frac{1}{v_g^o(\lambda_0 - \frac{\Delta\lambda_{0.5}}{2})} - \frac{1}{v_g^o(\lambda_0 + \frac{\Delta\lambda_{0.5}}{2})}. \tag{2}$$

For unchirped Gaussian pulses with a time–bandwidth product (TBP) of 0.44, a duration of 70 fs, and a center wavelength of 1.9 μm, the pulse's GVD in proustite is 200.14 fs/cm. Considering a crystal length L of 3.5 mm, the range of measurable pulse widths $\Delta\tau$ can be calculated as follows:

$$31\ \mathrm{fs} = \mathrm{L} \cdot \mathrm{GVD} \cdot \mathrm{TBP} < \Delta\tau < \mathrm{L} \cdot \mathrm{GVM} = 1938\ \mathrm{fs}. \tag{3}$$

This condition is met to ensure accurate pulse duration measurements in the range of 70 fs to 1 ps. The 3.5 mm Ag_3AsS_3 crystal provides a spectral resolution, calculated from the equation:

$$\delta\lambda_{\mathrm{calc}} = \frac{0.44\lambda_0}{L \cdot |n_o'(\lambda_0) - \frac{1}{2} \cdot n_e'(\frac{\lambda_0}{2})|}, \tag{4}$$

where $n'(\lambda) = \frac{dn}{d\lambda}$, and indices o and e refer to ordinary and extraordinary rays, respectively. The estimated spectral resolution $\delta\lambda_{\mathrm{calc}}$ is 2.7 nm at 1.9 μm, which allows accurate measurements of one picosecond duration pulse. A full beam divergence angle of 4.2° in the crystal yields 194 nm of spectral range. Thus, the selected crystal thickness allows the measurement of pulses with durations from 70 fs to 1 ps with wavelengths of 1.9 μm.

Optics EXPRESS

When accounting for the impact of pulse dispersion broadening during the propagation of USP, it's important to consider the group delay dispersion (GDD) introduced by the cylindrical lens and, biprism, in addition to that of the crystal. The maximum calculated GDD of the CL1 lens and Fresnel biprism is $-624.8\,\mathrm{fs}^2$, and the GDD of the SHG crystal when passing half of the crystal length is $893.9\,\mathrm{fs}^2$. The total GDD is $269.1\,\mathrm{fs}^2$, which introduces negligible changes in the characteristics of the measured pulse with a duration of about 70 fs. Thus, when a bandwidth-limited Gaussian pulse of 70 fs duration propagates through a medium with such a GDD, the output pulse duration will be 70.8 fs. However, this is only a rough estimate of the broadening of the unchirped Gaussian pulse, which does not take into account the complex spatial propagation through the optical components. Numerical modeling of the spatio-temporal propagation through the lens, biprism, and crystal will allow the effects of dispersion to be accurately determined.

A pair of cylindrical N-BK7 lenses CL2 and CL3 with focal lengths of 50 and 25 mm form a trace along the wavelength, and delay axis, respectively. At the rear focal plane of the CL3 lens is a filtering slit S which removes the collinear second harmonic component. A CS2100M-USB camera (Thorlabs Inc., USA) is used to record the traces, which has a sCMOS 2.1 MP silicon monochrome image sensor with a high dynamic range of up to 87 dB and 16-bit digital output.

The schematic of the experimental setup for validation of SHG trace measurements from FROG and GRENOUILLE, as well as autocorrelation and spectral traces, is shown in Fig. 2. A previously developed all-fiber thulium laser with an amplifier at 1.9 µm [28,29] is used as an ultrashort pulse source. The pulse repetition rate was 23.8 MHz and the pulse duration could be varied from 70 fs to 1 ps by tuning the polarization controller in the laser source. A reflective collimator RC08APC (Thorlabs Inc., USA) with a focal length of 33 mm was used for collimation of the radiation emitted from the laser fiber with a mode field diameter of about 20 µm. The diameter of the collimated laser beam was approximately 2 mm (yielding a total beam divergence $2\theta \approx 0.035°$). The use of an RC02APC reflective collimator (Thorlabs Inc, USA) with a 7 mm focal length, which provides a larger divergence ($2\theta \approx 0.152°$), resulted in some discrepancies between the FROG and GRENOUILLE traces of a complex pulse (see Appendix A), but simple Gaussian-shaped pulses were measured quite well [26].

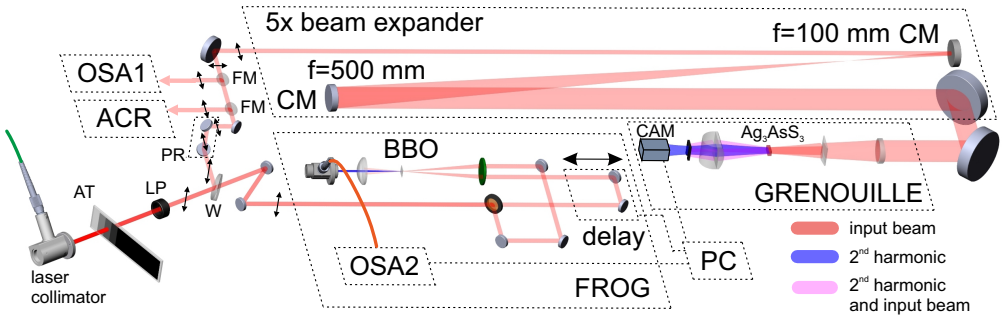

Fig. 2. Schematic of the experimental setup for simultaneous measurement of SHG traces from FROG and GRENOUILLE and autocorrelation and spectral traces. AT – variable attenuator. LP – linear polarizer. W – wedge. PR – polarization rotator. FM – flip mirror. OSA1 – Fourier spectrometer OSA207C (Thorlabs, USA). ACR – autocorrelator pulseCheck (APE Gmbh., Germany). CM – concave mirror. OSA2 – spectrometer AQ6370C (Yokogawa Ltd., Japan). CAM – camera CS2100M-USB (Thorlabs Inc., USA). PC – personal computer.

An attenuator AT was used to attenuate the signal in front of a linear polarizer LP due to its laser-induced damage threshold. The LP was used to extract only the vertical polarization because the output radiation of the laser system has random polarization. Most of the radiation

Optics EXPRESS

(85 %) passed through the CaF_2 wedge W and entered the homemade SHG-based FROG setup with a 0.6 mm thin BBO crystal. The GDD of the CaF_2 wedge is about $-95\,fs^2$, which does not introduce significant dispersion broadening in a 70 fs bandwidth-limited pulse (it broadens to 70.1 fs, i.e., by only 0.1%.). The FROG setup uses an AQ6370C spectrometer OSA2 (Yokogawa Ltd., Japan) together with a multimode silica fiber with a 105 μm core diameter to record the spectrum. The CaF_2 wedge W taps 15 % of the radiation for pulse characterization measurements using the GRENOUILLE device, autocorrelator ACR pulseCheck (APE Gmbh., Germany), OSA207C Fourier-transform spectrometer OSA1 (Thorlabs Inc., USA). The polarization of the radiation becomes horizontal after passing the polarization rotator PR, which is necessary for measurements on the autocorrelator and on the GRENOUILLE device due to the orientation of the crystal axes of these devices. Measurement on the spectrometer or autocorrelator is possible using flip mirrors FM, which prevents simultaneous measurement on the GRENOUILLE device.

Before reaching the GRENOUILLE device, the laser beam passes through a 5x beam expander consisting of two concave mirrors CM with focal lengths of 100 and 500 mm. The beam expander is necessary both to ensure the maximum possible delay between two overlapping pulses in the SHG crystal (see top view in Fig. 1(b)) and to fulfill the condition that the phase matching angle for the entire spectrum of incident pulses should be within the incidence angle of the focused beam (see side view in Fig. 1(b)). The calculated diameter of the laser beam at the entrance to the GRENOUILLE device is 20 mm at the $1/e^2$ level.

The paper presents the measurement results for three pulse generation regimes of the laser system by tuning the polarization controller and obtaining different pulse durations: 74.5 fs, 93.5 fs, 896.1 fs.

Calibration for GRENOUILLE was conducted prior to measuring each pulse generation regime. This process consists of determining the parameters of the wavelength-time grid on the sensor using an etalon distance [27,30]. Instead of an etalon, a double pulse obtained by the adjustment of the polarization controller of the laser system is used. The temporal and spectral characteristics of this pulse are determined using an autocorrelator and a spectrometer, which are used to calibrate the delay and wavelength axes of the device according to the procedure described in [30]. Since between the measurements of the two regimes with pulse durations of 74.5 and 93.5 fs and the 896.1 fs regime, the camera was removed from the experimental setup for another experiment and then returned back, the calibration results for these regimes are slightly different. The calibration results, the input power values to the devices, and the signal-to-noise ratios for the measured traces are presented in Table 1.

Table 1. The calibration results, the input power values to the devices, and the signal-to-noise ratios for the measured traces. N_t – number of time points, N_λ – number of wavelength points, $\delta\tau$ – time step, $\delta\lambda$ – wavelength step, λ_c – central wavelength, E_{in} – input pulse energy, SNR – signal-to-noise ratio.

Regime	Device	N_t	N_λ	$\delta\tau$, fs	$\delta\lambda$, nm	λ_c, nm	E_{in}, nJ	SNR, dB
896.1 fs	GRENOUILLE	1920	1080	2.1138	0.057	950.72	0.5	14
	FROG	3000	201	1.3343	0.34826	950	2.6	38
93.5 fs	GRENOUILLE	1920	1080	2.4429	0.0536	946.88	1.1	23
	FROG	2048	201	1.3343	0.34826	950	5.5	38
74.5 fs	GRENOUILLE	1920	1080	2.4429	0.052	947.03	1.1	22
	FROG	2048	201	1.3343	0.39801	950	5.6	33

When all components of the GRENOUILLE device are aligned, a slight asymmetry in the measured trace becomes noticeable when the pulse generation regime is changed. Since the GRENOUILLE device can be used for measuring spatial chirp [31], this trace asymmetry is presumably due to different spatial chirp due to the angled end of the fiber in the output of the

Optics EXPRESS

amplifier (FC/APC connector). GRENOUILLE measures spatial chirp by such trace asymmetry, and it can be used to re-align the laser setup to remove it [31]. Therefore, when changing the pulse generation regime, it was necessary to slightly adjust the input beam to the GRENOUILLE device to eliminate the asymmetry in the trace.

The single-shot measurement time for the GRENOUILLE trace is determined by the camera's exposure time and was set at 600 milliseconds. The (multi-shot) FROG measurement time depends on the number of delay points and the spectrum measurement time at each step. To obtain a delay span of about 4 ps without loss of temporal resolution in FROG requires more than 2000 spectra measurements, which at the resolution and sensitivity of the OSA2 spectrometer requires more than 20 minutes of FROG trace measurements, far exceeding the time required to measure the GRENOUILLE trace with the same span. It should be noted that the pulse generation regime strongly depends on the environmental parameters: temperature, vibration, and polarization controller settings. So during the time-consuming trace measurement with the FROG device, it was important to ensure that the regime does not change, which was done by monitoring the GRENOUILLE device trace.

3. Experimental results

Obtaining the intensity-and-phase curves from measured traces requires a retrieval algorithm. In this work, the RANA approach is used for this procedure, which allows the retrieval of complex pulses with high accuracy and reliability [32]. Before retrieving the pulses from the traces, the measured GRENOUILLE and FROG traces were linearly interpolated into a grid of 4096 by 4096 points with a frequency step of ≈ 48.7 GHz and a time step of ≈ 5 fs to achieve a sufficiently high resolution in the frequency and time domains. Interpolation was performed in such a way that, in the time and frequency domains outside the measurement limits all values of the traces were set to zero, as usual. The retrieving time for such large traces is on the order of 30 min. To estimate the results of retrieval by the RANA approach, both the G error and G′ error were used. The G error is defined as the root mean square between measured and retrieved traces, while the G′ error is normalized by the trace area, rather than the number of points [27,32]. Table 2 summarizes the retrieving errors of FROG and GRENOUILLE traces obtained by the RANA algorithm. The pulse generation regime name was determined from the pulse duration obtained from the FROG trace pulse-retrieval results and will be used as such hereafter. In the case of the 74.5 fs pulse duration, an intensity mask was used for the GRENOUILLE trace, which will be described in the corresponding subsection.

Table 2. Retrieved pulse durations $\Delta\tau$ and spectrum widths $\Delta\lambda_{0.1}$, G and G′ errors from the FROG and GRENOUILLE traces. $\Delta\lambda_{0.1}^{\mathrm{OSA1}}$ is the spectrum width at 0.1 of the maximum measured by OSA1. RE - relative error of the pulse duration from the GRENOUILLE trace with respect to the pulse duration from the FROG trace. The asterisk, *, indicates results obtained with the applied mask. Note that all results indicate excellent convergence of the algorithm, as well as highly stable pulses in the case of the multi-shot FROG measurements.

$\Delta\lambda_{0.1}^{\mathrm{OSA1}}$, nm	FROG				GRENOUILLE				
	$\Delta\tau$, fs	$\Delta\lambda_{0.1}$, nm	G error	G′ error	$\Delta\tau$, fs	$\Delta\lambda_{0.1}$, nm	G error	G′ error	RE, %
72.2	896.1	73.4	0.00344	0.151	892.1	75.7	0.00275	0.146	0.4
85.4	93.5	89.6	0.0006	0.068	94	89.5	0.00121	0.136	0.5
115.4	74.5	105.7	0.00168	0.148	80.6 77.5*	119.9 110.2*	0.00239 0.0020*	0.248 0.189*	8.2 4*

In all cases, the GRENOUILLE retrieval error is approximately the same and indicative of good retrieval and a good measurement. For a pulse duration of 896.1 fs, the FROG recovery error closely matches that of GRENOUILLE, while for 93.5 fs, the FROG recovery error is

Optics EXPRESS

half as much. There were minimal power and polarization fluctuations in the measurement of the generation regime characteristics with a duration of 93.5 fs, expressed in the smoothness of the trace measurement. This indicates that GRENOUILLE complements FROG in yielding short-term or even single-shot pulse measurements, whereas FROG (when scanned) averages over more pulses and so reveals pulse-train instability by a somewhat smeared trace, as has been shown previously [33].

In order to quantitatively compare the retrieval results from the FROG and GRENOUILLE traces, Pearson correlation coefficients were calculated and are presented in Table 3.

Table 3. Pearson correlation coefficients for spectral and temporal intensities retrieved from the FROG and GRENOUILLE traces.

Data	896.1 fs	93.5 fs	74.5 fs w/o mask	74.5 fs w. mask
Temp. intensity from GREN. & Temp. intensity from FROG	0.967	0.999	0.992	0.996
Sp. intensity from GREN. & Meas. sp.	0.962	0.845	0.894	0.949
Sp. intensity from FROG & Meas. sp.	0.946	0.845	0.932	0.932
Sp. intensity from GREN. & Sp. intensity from FROG	0.967	0.904	0.921	0.954

3.1. 896.1 fs pulse

Figure 3 shows the results of measured GRENOUILLE and FROG traces of the pulse with a duration of about 896.1 fs. Figures 3(a), (b), and (c) show the measured GRENOUILLE trace, the retrieved trace, and the difference between the measured and retrieved traces, respectively. In general, the recovery result is excellent, and the structures of the measured and recovered traces are similar. The pulse has a significant chirp and broad spectral width and is not bandwidth limited (Fig. 3(e)), so some difference in the measured and retrieved GRENOUILLE traces can be attributed to the limitation of the spectral range of the GRENOUILLE device. Nevertheless, the measurement results are in good agreement with the results obtained by the FROG setup which is shown in Table 3. The error of the GRENOUILLE pulse duration measurement with respect to the FROG is 0.4%, which is generally considered excellent agreement for such a complex pulse. Finally, the FROG measurement shows some smearing, indicative of some drift in the pulse shape over the measurement, and effect not present in the GRENOUILLE trace, which was much faster. Comparison of the spectra measured by the spectrometer and those obtained from FROG and GRENOUILLE measurements also shows good agreement (Fig. 3(f)).

3.2. 93.5 fs pulse

Figure 4 shows the results for measuring a pulse with a duration of 93.5 fs, in the same form as for an 896.1 fs pulse. The intensity and phase characteristics obtained by the two devices agree well (as shown in Fig. 4(e)), as validated by high Pearson correlation coefficients. The spectral characteristics are also close (Fig. 4(f)). The error of the pulse duration obtained by the GRENOUILLE method with respect to the FROG method is 0.5%. The different slope of the pulse phase in the spectral and time domains is due to the slightly different displacement of the central wavelength of the pulses from the center of the spectral window in the GRENOUILLE and FROG measurement traces (Fig. 4(e),(f)). It can be seen that the intensity of the GRENOUILLE trace at the spectral edges is somewhat less than that of the FROG trace (Fig. 4(a),(d)), which is due to the limitation of the spectral width of the GRENOUILLE measurements, likely due to insufficiently tight focusing into the nonlinear crystal, but the RANA pulse-retrieval algorithm realizes this due to information elsewhere in the measured trace (specifically, at small delays) and appropriately enhances these components (Fig. 4(b),(c)).

Optics EXPRESS

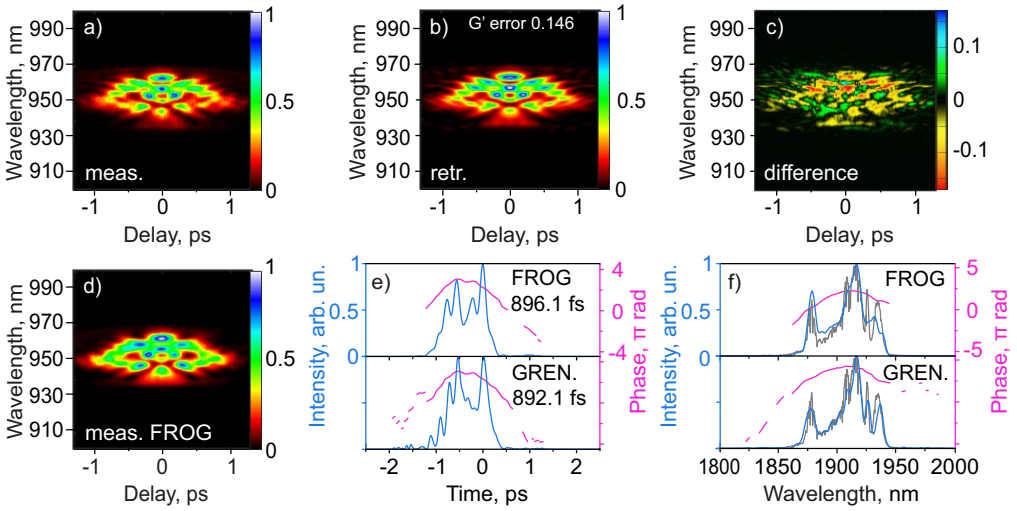

Fig. 3. Measured and retrieved results of 896.1 fs pulse on GRENOUILLE and FROG traces: (a) measured GRENOUILLE trace; (b) retrieved GRENOUILLE trace, (c) difference between measured and retrieved GRENOUILLE traces, (d) measured FROG trace; retrieved temporal (e) and spectral (f) intensity/phase from GRENOUILLE and FROG traces are shown in blue/pink. The gray curve shows the measured spectrum obtained with the OSA1.

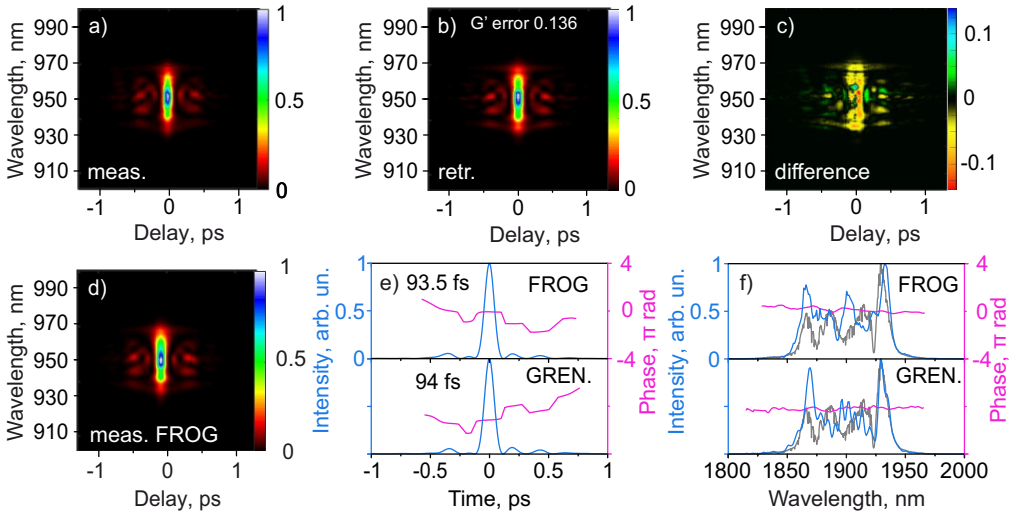

Fig. 4. Measured and retrieved results of 93.5 fs pulse on GRENOUILLE and FROG traces: (a) measured GRENOUILLE trace; (b) retrieved GRENOUILLE trace, (c) difference between measured and retrieved GRENOUILLE traces, (d) measured FROG trace; retrieved temporal (e) and spectral (f) intensity/phase from GRENOUILLE and FROG traces are shown in blue/pink. The gray curve shows the measured spectrum obtained with the OSA1.

3.3. 74.5 fs pulse

In this section, we summarize the measurement results of the shortest pulse with a duration of 74.5 fs. The pulse has a spectral FWHM of 85.2 nm that is wider than the previous ones, and obtaining the GRENOUILLE trace without special processing leads to a large error in the

Optics EXPRESS

pulse duration of about 8 %. By comparing the measured traces of GRENOUILLE (Fig. 5(a)) and FROG (Fig. 5(d)), it can be clearly seen that the intensity of spectral components in the wavelength region below 940 and above 960 nm in GRENOUILLE is less than that in FROG. To increase the intensity in these areas, a special mask can be applied that takes into account the intensity distribution of the input laser beam, the thickness of the crystal, and the beam crossing angle $\approx 5^\circ$ [34]. For the thick crystal used in GRENOUILLE, the mask is defined as the convolution of the spatial profile with itself over the beam region. The spatial distribution of the beam at the entrance to GRENOUILLE was determined by solving the equations in the paraxial approximation starting from the fiber. The spatial distribution of the beam is given by a Gaussian function with a diameter of 20 mm at the $1/e^2$ level. Applying the mask consists of dividing the values of the measured trace by the values of the resulting mask.

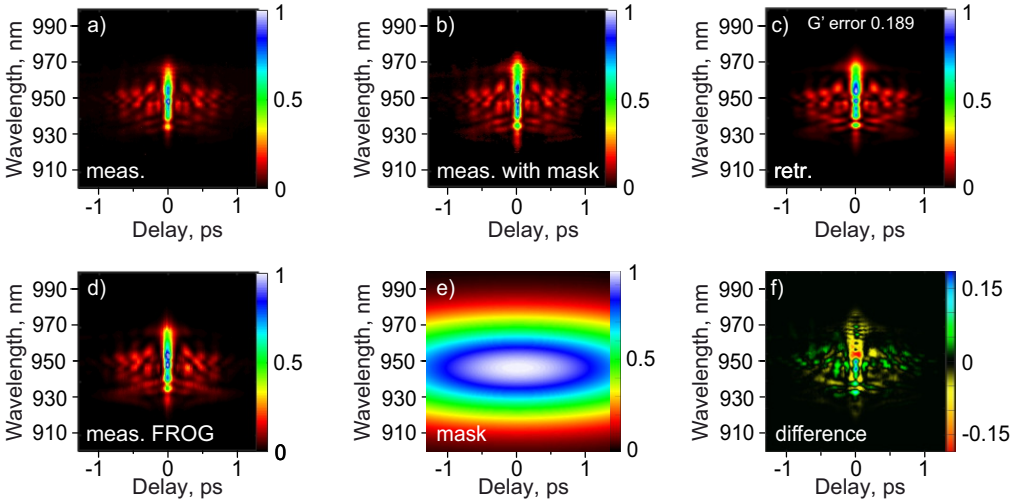

Fig. 5. Traces of 74.5 fs pulse with GRENOUILLE and FROG device: (a) measured GRENOUILLE trace, (b) measured GRENOUILLE trace with mask application, (c) retrieved trace for the measured GRENOUIILE trace with mask application, (d) measured FROG trace; (e) intensity mask for a 20 mm Gaussian beam; (f) difference between measured b) and retrieved c) traces.

After low-pass filtering of the measured GRENOUILLE trace, necessary to remove high-frequency digital noise from it, and applying the mask shown in Fig. 5(e), the GRENOUILLE trace has the appearance shown in Fig. 5(b). The trace intensities in the wavelength region longer than 960 and shorter than 940 nm increased, resulting in a decrease in the extracted pulse duration as well as a decrease in the retrieval error. This resulted in the trace becoming closer to the FROG trace. Figure 5(f) shows the difference between the trace with the applied mask Fig. 5(b) and the retrieved trace Fig. 5(c).

Figure 6(a) shows the retrieved temporal intensity and phase of 74.5 fs pulse by using FROG trace, GRENOUILLE trace, and GRENOUILLE trace with the mask. Without applying the mask, the pulse duration was 80.6 fs. The total error of pulse duration determined by the GRENOUILLE trace with the mask (77.5 fs) compared with the FROG trace is 4%.

The spectral intensities and phases for the FROG, GRENOUILLE, and GRENOUILLE with the mask measurements are shown in Fig. 6(b). The application of the mask caused the intensity of the spectrum to be closer to the measured spectrum. This is verified by the increase in the Pearson correlation coefficient of the measured spectrum and the spectral intensity obtained by retrieving the GRENOUILLE trace with the applied mask, see the second row in Table 3. Thus,

Optics EXPRESS

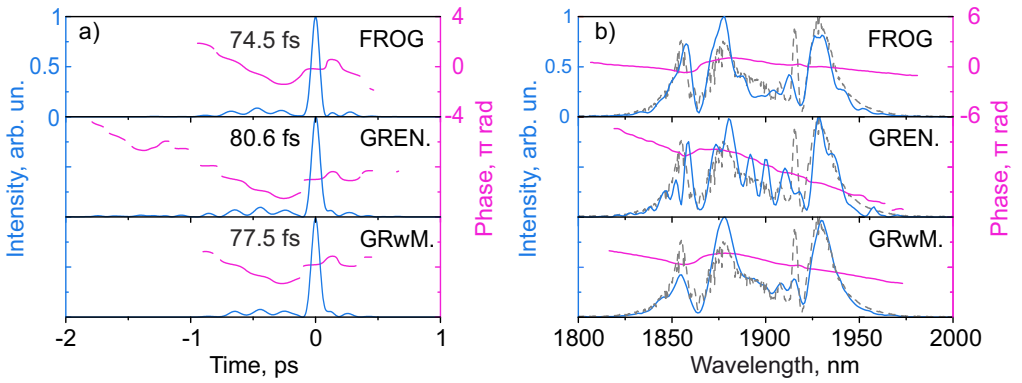

Fig. 6. Retrieved temporal (a) and spectral (b) intensity/phase profiles from the FROG, GRENOUILLE, and GRENOUILLE with mask traces, represented in blue/pink. The gray dotted curve shows the measured spectrum obtained with the OSA1.

the application of the mask reduced the pulse duration and brought the spectral intensity closer to the measured one, making the GRENOUILLE trace closer to the FROG trace.

4. Discussion

One of the estimates of trace measurement accuracy is the retrieval error. The retrieval error in GRENOUILLE is slightly larger than in FROG, so it can be argued that GRENOUILLE is less accurate than FROG. This is because, since GRENOUILLE uses a thick nonlinear crystal as a dispersing element, its spectral resolution is lower than that of FROG, which uses a thin crystal and spectrometer (ones of nm vs. tenths of nm). However, even the resolution in ones of nanometers is sufficient to characterize USP after applying modern approaches (RANA) to the trace reconstruction [32], so this is not a significant source of error in the results. This is confirmed by the Pearson correlation coefficients, which are close to one in all cases.

Some of the discrepancies in the measured FROG and GRENOUILLE traces may also be due to the instability of the pulse generation regime since the FROG trace was measured for more than 20 min, while the GRENOUILLE trace was measured for only 600 ms. The undoubted advantage of the GRENOUILLE system is its measurement speed, which allows it to monitor changes in the pulse generation regime of ultrafast fiber lasers. The slightly insufficient efficiency of SHG at the sides of the GRENOUILLE trace can be further reduced by changing the optical system, including, increasing the beam diameter at the input and decreasing the focal length of the cylindrical lens focusing the radiation into the nonlinear crystal. This would negate the need for a mask for broad-spectrum pulses.

SHG trace in GRENOUILLE can be distorted by aberrations as well as spatial chirp and pulse front tilt, and the nature of the distortions can be misidentified [35]. In our study, the SHG trace obtained with the GRENOUILLE device was validated with the SHG trace from multi-shot FROG, and for our experimental setup, no influence of possible aberrations on the trace was observed because the traces were very close. Furthermore, as shown in our study, beam divergence can affect the SHG trace, and numerical modelling of the spatio-temporal propagation of the pulse in the GRENOUILLE instrument is required to fully determine the optimal beam parameters as well as the influence of aberrations.

Regarding device sensitivity, the quantum efficiency of the silicon sCMOS sensors used in the research decreases by a factor of 7 from the maximum in the 950 nm region, which makes the sensitivity in measuring the traces of SHG pulses with a wavelength of 1.9 μm very important.

Optics EXPRESS

Nevertheless, even without the use of special mathematical methods, we were able to measure pulses with an energy of 500 pJ with a signal-to-noise ratio of 14 dB.

The LP at the output of the amplifier was used (see Fig. 2), so in this study, the characteristics of the USPs were measured only for linearly polarized pulses, as the autocorrelator and FROG usually do. GRENOUILLE can be used to measure the polarization-shaped pulses in our experimental setup by taking three SHG trace measurements at different positions of the LP (typically 0°, 45°, and 90°) and obtaining the characteristics of the pulses with time-varying polarization using the TURTLE method [36,37].

5. Conclusion

The developed GRENOUILLE system successfully measured USP from 74 to 900 fs at 1.8 to 2 μm with high speed (600 ms, not including the pulse retrieval procedure). It was shown that a mask was necessary for 74 fs pulse measurements due to the broad spectral bandwidth of the pulse. The GRENOUILLE measurement results were validated with the multi-shot FROG measurements and are in good agreement, as indicated by correlation coefficients close to one. Comparing the pulse durations obtained from the GRENOUILLE and FROG SHG traces, the error for the shorter pulses increased from 0.4 % for 896.1 fs to 4% for 74.5 fs in accordance with the increase in spectrum bandwidth. The effect of the laser beam divergence on the quality of the GRENOUILLE SHG trace was also shown. It was found that at an input beam divergence of 0.035° the SHG trace is close to the SHG trace of the multi-shot FROG. In order to analyse in more detail the requirements for beam characteristics at the input as well as the influence of aberrations, numerical simulations of the spatio-temporal propagation of the GRENOUILLE device could be performed in the future. In addition, further research could be directed towards the high speed measurement of polarisation-shaped pulses using the developed GRENOUILLE device and TURTLE method.

Appendix A: GRENOUILLE trace measurements of the complex pulse with the 7 mm focal length collimator

In [26], it was shown the measurement results with a reflective collimator RC02APC with a focal length of 7 mm to input USPs into the developed GRENOUILLE device. The spectrum and autocorrelation trace obtained by the GRENOUILLE device were in good agreement for Gaussian-shaped pulses with the data measured by OSA1 and ACR, respectively, [26]. However, the measured results of the complex pulses were slightly different. This raised a hypothesis about the laser divergence requirements at the input to the GRENOUILLE device for measuring complex-shaped pulses.

Figure 7 shows the measured and retrieved FROG and GRENOUILLE traces of the complex pulse with a 58.8 nm spectral FWHM and 62 fs duration with the RC02APC reflective collimator and a camera with a Sony ICX-829AL sensor (Sony Inc., Japan). As can be seen, there is a mismatch between the sides of the measured FROG (Fig. 7(a)) and GRENOUILLE (Fig. 7(b)) traces. Despite the relatively large error in the FROG trace reconstruction due to the instability of the pulse generation regime during measurement, the structure of the reconstructed FROG trace (Fig. 7(c)) is close to that of the measured trace. The side and central parts of the resulting GRENOUILLE (Fig. 7(d)) have different intensity and structure compared to the measured trace. Presumably, these discrepancies are due to the large beam divergence ($2\theta \approx 0.152°$) after the collimator and correspondingly small radius of curvature of the wavefront at the entrance to the GRENOUILLE device.

So, in order to increase the validity of the GRENOUILLE device, it was necessary to reduce the radiation divergence by using a reflective collimator with a larger focal length. With the installation of a reflective collimator providing a total beam divergence of $2\theta \approx 0.035°$, the FROG and GRENOUILLE traces became close. Thus, a 4.3-fold decrease in the radiation divergence (from

Optics EXPRESS

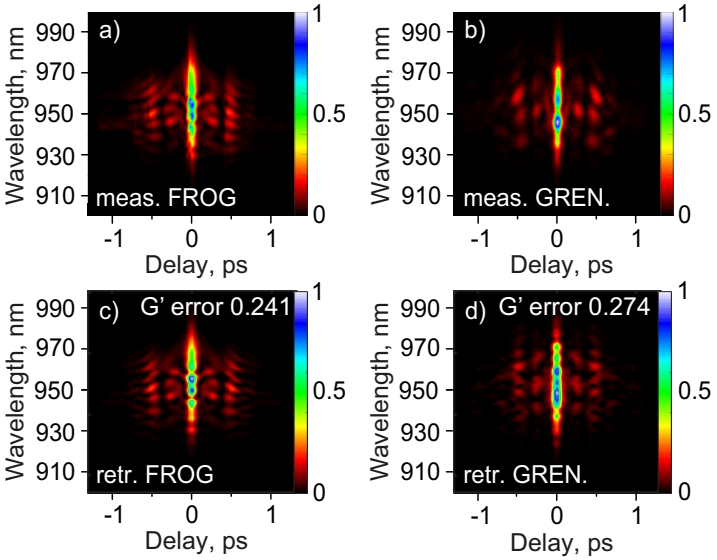

Fig. 7. Measured (a,b) and retrieved (c,d) FROG and GRENOUILLE traces, respectively.

0.152° to 0.035°) was sufficient to bring the results of FROG and GRENOUILLE measurements closer to each other, but a detailed modeling of the radiation propagation is necessary for a more accurate assessment.

Funding. The research work was supported by the Priority 2030 program proposed by Bauman Moscow State Technical University.

Acknowledgments. We would like to thank Andrey Bushunov for the camera provided, endless interest in our work and fruitful discussions.

Disclosures. Rick Trebino owns a company that sells pulse-measurement devices, and Selcuk Akturk and Rana Jafari consult for it.

Data availability. Data underlying the results presented in this paper are not publicly available at this time but may be obtained from the authors upon reasonable request.

References

1. Y. Xie, R. Long, Z. Ma, *et al.*, "1.7 μm sub-200 fs vortex beams generation from a thulium-doped all-fiber laser," Opt. Express **31**(17), 27858–27867 (2023).
2. D. Xu, K. N. Bourdakos, A. Crisford, *et al.*, "All-fiberized 1840-nm femtosecond thulium fiber laser for label-free nonlinear microscopy," Biomed. Opt. Express **14**(9), 4520–4530 (2023).
3. H. Ahmad, M. Azri, R. Ramli, *et al.*, "2 μm passively mode-locked thulium-doped fiber lasers with Ta_2AlC-deposited tapered and side-polished fibers," Sci. Rep. **11**(1), 21278 (2021).
4. C. W. Rudy, M. J. Digonnet, and R. L. Byer, "Advances in 2-μm Tm-doped mode-locked fiber lasers," Opt. Fiber Technol. **20**(6), 642–649 (2014).
5. J. A. Curcio and C. C. Petty, "The near infrared absorption spectrum of liquid water," J. Opt. Soc. Am. **41**(5), 302–304 (1951).
6. P. Elahi, H. Kalaycioğlu, Ö. Akçaalan, *et al.*, "Burst-mode thulium all-fiber laser delivering femtosecond pulses at a 1 GHz intra-burst repetition rate," Opt. Lett. **42**(19), 3808–3811 (2017).
7. D. C. Sordillo, L. A. Sordillo, P. P. Sordillo, *et al.*, "Short wavelength infrared optical windows for evaluation of benign and malignant tissues," J. Biomed. Opt. **22**(4), 045002 (2017).
8. Y. Tang, L. G. Wright, K. Charan, *et al.*, "Generation of intense 100 fs solitons tunable from 2 to 4.3 μm in fluoride fiber," Optica **3**(9), 948–951 (2016).
9. S. Xing, A. S. Kowligy, D. M. Lesko, *et al.*, "All-fiber frequency comb at 2 μm providing 1.4-cycle pulses," Opt. Lett. **45**(9), 2660–2663 (2020).
10. S. Xing, D. Lesko, T. Umeki, *et al.*, "Single-cycle all-fiber frequency comb," APL Photonics **6**(8), 086110 (2021).
11. V. Voropaev, S. Xie, A. Donodin, *et al.*, "Octave-Spanning Supercontinuum Generation in As_2S_3–Silica Hybrid Waveguides Pumped by Thulium-Doped Fiber Laser," J. Lightwave Technol. (2023).

Optics EXPRESS

12. S. Salalykin, D. Batov, V. Voropaev, *et al.*, "Raman soliton generation in germanosilicate fibers pumped at 1.9 μm," in *Frontiers in Optics*, (Optica Publishing Group, 2022), pp. JTu5B–34.
13. R. A. Richter, N. Tolstik, and I. T. Sorokina, "Efficient high-energy Raman soliton generation in a Tm: doped large mode area fiber amplifier," Opt. Express **30**(3), 3329–3344 (2022).
14. V. V. Dvoyrin and I. T. Sorokina, "All-fiber optical supercontinuum sources in 1.7-3.2 μm range," in *Fiber Lasers XI: Technology, Systems, and Applications*, vol. 8961 (SPIE, 2014), pp. 247–251.
15. B. Voisiat, D. Gaponov, P. Gečys, *et al.*, "Material processing with ultra-short pulse lasers working in 2 μm wavelength range," in *Laser Applications in Microelectronic and Optoelectronic Manufacturing (LAMOM) XX*, vol. 9350 (SPIE, 2015), pp. 120–127.
16. R. Richter, N. Tolstik, and I. T. Sorokina, "In-bulk silicon processing with ultrashort pulsed lasers: three-photon-absorption versus two-photon-absorption," in *Mid-Infrared Coherent Sources*, (Optica Publishing Group, 2018), pp. MW4C–2.
17. M. Gebhardt, T. Heuermann, Z. Wang, *et al.*, "Soft x-ray high order harmonic generation driven by high repetition rate ultrafast thulium-doped fiber lasers," in *Fiber Lasers XVII: Technology and Systems*, vol. 11260 (SPIE, 2020), pp. 84–89.
18. M. Gebhardt, C. Gaida, F. Stutzki, *et al.*, "Multi-GW, 100 fs thulium-doped fiber laser system for high-harmonic generation at high repetition rates," in *The European Conference on Lasers and Electro-Optics*, (Optica Publishing Group, 2017), p. CJ_11_1.
19. K. Scholle, S. Lamrini, P. Koopmann, *et al.*, "2 μm laser sources and their possible applications," in *Frontiers in guided wave optics and optoelectronics*, (IntechOpen, 2010).
20. D. Tomaszewska-Rolla, R. Lindberg, V. Pasiskevicius, *et al.*, "A comparative study of an Yb-doped fiber gain-managed nonlinear amplifier seeded by femtosecond fiber lasers," Sci. Rep. **12**(1), 404 (2022).
21. A. Rampur, Y. Stepanenko, G. Stępniewski, *et al.*, "Ultra low-noise coherent supercontinuum amplification and compression below 100 fs in an all-fiber polarization-maintaining thulium fiber amplifier," Opt. Express **27**(24), 35041–35051 (2019).
22. R. Trebino, R. Jafari, S. Akturk, *et al.*, "Highly reliable measurement of ultrashort laser pulses," J. Appl. Phys. **128**(17), 171103 (2020).
23. P. O'Shea, M. Kimmel, X. Gu, *et al.*, "Highly simplified device for ultrashort-pulse measurement," Opt. Lett. **26**(12), 932–934 (2001).
24. S. Akturk, M. Kimmel, P. O'Shea, *et al.*, "Extremely simple device for measuring 20-fs pulses," Opt. Lett. **29**(9), 1025–1027 (2004).
25. S. Akturk, M. Kimmel, and R. Trebino, "Extremely simple device for measuring 1.5-μm ultrashort laser pulses," Opt. Express **12**(19), 4483–4489 (2004).
26. D. Vlasov, V. Voropaev, D. Batov, *et al.*, "Ultrashort Pulse Measurement at 1.9 μm Using GRENOUILLE Technique," in *Frontiers in Optics*, (Optica Publishing Group, 2021), pp. JTu1A–37.
27. R. Trebino, *Frequency-Resolved Optical Gating: The Measurement of Ultrashort Laser Pulses: The Measurement of Ultrashort Laser Pulses* (Springer Science & Business Media, 2002).
28. A. Donodin, V. Voropaev, D. Batov, *et al.*, "Numerical model of hybrid mode-locked Tm-doped all-fibre laser," Sci. Rep. **10**(1), 17396 (2020).
29. V. Voropaev, D. Batov, A. Voronets, *et al.*, "All-fiber ultrafast amplifier at 1.9 μm based on thulium-doped normal dispersion fiber and LMA fiber compressor," Sci. Rep. **11**(1), 23693 (2021).
30. B.-K. Yang, H. S. Rho, J. M. Seo, *et al.*, "Design, construction and calibration of a grenouille, single-shot, ultrashort-pulse measurement system," J. Korean Phys. Soc. **52**(2), 269–274 (2008).
31. S. Akturk, M. Kimmel, P. O'Shea, *et al.*, "Measuring spatial chirp in ultrashort pulses using single-shot frequency-resolved optical gating," Opt. Express **11**(1), 68–78 (2003).
32. R. Jafari, T. Jones, and R. Trebino, "100% reliable algorithm for second-harmonic-generation frequency-resolved optical gating," Opt. Express **27**(3), 2112–2124 (2019).
33. M. Rhodes, G. Steinmeyer, J. Ratner, *et al.*, "Pulse-shape instabilities and their measurement," Laser Photonics Rev. **7**(4), 557–565 (2013).
34. D. Lee, Z. Wang, X. Gu, *et al.*, "Effect-and removal-of an ultrashort pulse's spatial profile on the single-shot measurement of its temporal profile," J. Opt. Soc. Am. B **25**(6), A93–A100 (2008).
35. C. Pichette, M. Piché, P. Marquet, *et al.*, "Study of the impact of wavefront aberrations on the characterization of ultrashort laser pulses with GRENOUILLE," J. Opt. Soc. Am. A **39**(8), 1489–1497 (2022).
36. L. Xu, P. Schlup, O. Masihzadeh, *et al.*, "Analysis of the measurement of polarization-shaped ultrashort laser pulses by tomographic ultrafast retrieval of transverse light E fields," J. Opt. Soc. Am. B **26**(12), 2363–2369 (2009).
37. P. Schlup, O. Masihzadeh, L. Xu, *et al.*, "Tomographic retrieval of the polarization state of an ultrafast laser pulse," Opt. Lett. **33**(3), 267–269 (2008).